Appl Phys A (2009) 97: 167–177
DOI 10.1007/s00339-009-5256-5

Applied Physics A
Materials Science & Processing

Nanostructures and magnetic properties of cobalt ferrite ($CoFe_2O_4$) fabricated by electrospinning

Montana Sangmanee · Santi Maensiri

Received: 27 August 2008 / Accepted: 14 April 2009 / Published online: 16 May 2009

Abstract This paper describes the fabrication of cobalt ferrite ($CoFe_2O_4$) nanostructures (in the form of nanofibers and nanoparticles) by the electrospinning method using a solution that contained poly(vinyl pyrrolidone) (PVP) and cheap Co and Fe nitrates as metal sources. The as-spun and calcined $CoFe_2O_4$/PVP composite samples were characterized by TG-DTA, X-ray diffraction, FT-IR, SEM and TEM, respectively. After calcination of the as-spun $CoFe_2O_4$/PVP composite nanofibers (fiber size of 320 ± 48 nm in diameter) at 500, 600, and 800°C in air for 3 h with different heating rates of 5 or 20°C/min, either $NiFe_2O_4$ nanofibers of ∼10−200 nm in diameter or nanoparticles with particle sizes of ∼50−400 nm having a well-developed spinel structure were successfully obtained. The crystal structure and morphology of the nanofibers were influenced by the calcination temperature and heating rate. A faster heating rate allowed for a rapid removal of the PVP matrix and resulted in a complete change from fibrous structure to particle in the calcined $CoFe_2O_4$/PVP composite nanofibers. Room temperature magnetization results showed a ferromagnetic behavior of the calcined $CoFe_2O_4$/PVP composite nanofibers, having their hysteresis loops in the field range of ±4500 and 3000 Oe for the samples calcined respectively with heating rates of 5 and 20°C/min. The values of the specific magnetization (M_s) at 10 kOe, remnant magnetization (M_r), M_r/M_s ratio, and coercive forces (H_c) are obtained from hysteresis loops. It was found that the values of M_s, M_r, M_r/M_s, and H_c depended strongly on morphology of the $CoFe_2O_4$ nanostructures.

PACS 75.50.Tt · 75.75.-a · 81.07.Bc · 81.10.-h

1 Introduction

Spinel ferrites with the general formula AFe_2O_4 (e.g. A = Mn, Co, Ni, Cu, Zn) are a very important group of magnetic materials because of their interesting magnetic and electrical properties with chemical and thermal stabilities. These materials are technologically important and have been used in many applications including magnetic recording media and magnetic fluids for the storage and/or retrieval of information, magnetic resonance imaging (MRI) enhancement, catalysis, magnetically guided drug delivery, sensors, pigments, etc. [1–3]. Cobalt ferrite ($CoFe_2O_4$) is one of the most important spinel ferrites having an inverse spinel structure where oxygen atoms make up an FCC lattice and one half of Fe^{3+} ions occupies the tetrahedral A sites and the other half, together with Co^{2+} ions locate at the octahedral B sites [3]. It is ferromagnetic with a Curie temperature (T_C) around 793 K and shows a relative large magnetic hysteresis which distinguishes it from other spinel ferrites. Recently, $CoFe_2O_4$ has attracted considerable attention due to their large magnetocrystalline anisotropy, high coercivity, moderate saturation magnetization, large magnetostrictive coefficient, chemical stability and mechanical hardness [3]. These attractive properties make it a good candidate for various applications such as high density recording media [4–6] and

M. Sangmanee · S. Maensiri
Small & Strong Materials Group (SSMG), Department of Physics, Faculty of Science, Khon Kaen University, Khon Kaen, 40002, Thailand

M. Sangmanee
e-mail: sanmae@kku.ac.th

S. Maensiri (✉)
Integrated Nanotechnology Research Center (INRC), Faculty of Science, Khon Kaen University, Khon Kaen, 40002, Thailand
e-mail: santimaensiri@gmail.com
Fax: +66-43-202374

magnetic fluids [7]. Cobalt ferrite nanoparticle has been also known to be a photomagnetic material which shows an interesting light-induced coercivity change [8, 9] and as active material for lithium ion battery [10, 11].

Various nanostructures of $CoFe_2O_4$ such as nanoparticles, nanowires and nanorods have been successfully fabricated by hydrothermal method [12], co-precipitation [13] and thermal decomposition [14], pulsed laser deposition [15], electrodepositon [16], and chemical method [17]. In recent years, the ordered magnetic materials such as nanorods and nanowires have attracted a great interest due to their enhanced magnetic property [16, 18]. Nanofiberization of magnetic materials would be also of great interest and will expand their technological application in many areas including nanocomposites, nanosensors, nano-electronics and photonics. Electrospinning represents a simple and convenient method for preparing polymer fibers and ceramic fibers with both solid and hollow interiors that are exceptionally long in length, uniform in diameter ranging from tens of nanometers to several micrometers, and diversified in compositions [19–22]. In an electrospinning process [23–26], an electrical potential is applied between a droplet of a polymer solution held at the end of the nozzle of the spinneret and a grounded target. When the applied electric field overcomes the surface tension of the droplet, a charged jet of polymer solution is ejected. The route of the charged jet is controlled by the electric field. The jet exhibits bending instabilities caused by repulsive forces between the charges carried with the jet. The jet extends through spiraling loops. As the loops increase in diameter the jet grows longer and thinner until it solidifies or it is collected on the target. Some novel metal oxide nanofibers e.g. TiO_2 [27, 28], V_2O_5 [29], and ZnO [30], and oxide ceramic compounds e.g. $NiCo_2O_4$ [31], $MgTiO_3$ [32], $LiMn_2O_4$ [33], $Pb(Zr_{0.52}Ti_{0.48}O_3$ [34], $NaCo_2O_4$ [35], $Ba_{0.6}Sr_{0.4}TiO_3$ [36], and $Bi_{3.15}Nd_{0.85}Ti_3O_{12}$) [37] have been successfully prepared by electrospinning process followed by calcination at high temperature. So far, only a few studies report on electrospinning of magnetic oxide nanofibers. The first study on the fabrication of electrospun $NiFe_2O_4$ nanofibers was reported by Li et al. [38]. In their study polycrystalline nanofibers of $NiFe_2O_4$ with an average diameter of 46 nm were prepared by electrospinning a solution that contained poly(vinyl pyrrolidone) (PVP) and alkoxide precursors to nickel and iron oxides, followed by hydrolysis and calcination at 550°C in air. However, metal alkoxide precursors used in their study are expensive and may not be suitable for large scale production. Moreover, solution preparation for electrospinning must be carried out in glove box to prevent oxidation of the metal alkoxide precursors. Recently, our group have successfully fabricated $CuFe_2O_4$ nanofibers (60–200 nm in diameter with specific saturation magnetization (M_s) values of 17.73–23.98 emu/g) and $MgFe_2O_4$ nanofibers (~100 nm in diameter with specific saturation magnetization (M_s) value of 17.00 emu/g) by electrospinning using a solution that contained poly(vinyl pyrrolidone) and cheap metal nitrates as alternative metal sources [39, 40]. The use of alternative precursor without the need of glove box or special procedures offers the more convenient and possibly more preferable method for preparation of a solution for electrospinning.

In this paper, we report the fabrication of $CoFe_2O_4$ nanostructures (in the forms of nanofibers and nanoparticles) by electrospinning using a solution that contained poly(vinyl pyrrolidone) and cheap metal nitrates of Co and Fe. The fabricated $CoFe_2O_4$ samples were characterized by TG-DTA, XRD, FTIR, SEM, and TEM. The magnetic properties of prepared $CoFe_2O_4$ samples were investigated using a vibrating sample magnetometer (VSM) at room temperature. The effects of calcination temperature and heating rate on morphology, structure, and magnetic properties of the fabricated $CoFe_2O_4$/PVP composite samples were also studied.

2 Experimental section

In this study, $Co(NO_3)_2{\cdot}6H_2O$ (99.95% purity, Kanto Chemicals, Japan), $Fe(NO_3)_3{\cdot}9H_2O$ (99.99% purity, Kanto Chemicals, Japan) and polyvinyl pyrrolidone (PVP) (M_n = 1,300,000, Aldrich), N,N-Dimetylformamide (DMF) (99.8% purity, Fluka, Switzerland), acetic acid (100% purity, BDH, England), and ethanol (100% purity, BDH, England) were used as the starting chemicals. In the preparation of the solution for electrospinning, we used a solution that contained poly(vinyl pyrrolidone) mixed with $Co(NO_3)_2{\cdot}6H_2O$ and $Fe(NO_3)_3{\cdot}9H_2O$. A PVP/ethanol solution, was prepared using a ratio of 1.0 g PVP to 9 ml ethanol. A metal nitrates/DMF solution was prepared by dissolving 0.01 mol $Co(NO_3)_2{\cdot}6H_2O$ and 0.02 mol $Fe(NO_3)_3{\cdot}9H_2O$) in 10 ml of DMF and stirred for 5 h. Subsequently, the metal nitrates/DMF solution (0.8 ml) was added slowly to the PVP/ethanol solution (10 ml) under vigorous stir at 27°C for 5 h to obtain a well-dissolved solution. This final solution was used for electrospinning.

The prepared polymer solution was loaded into a plastic syringe equipped with a 22-gauge needle made of stainless steel. The electrospinning process was carried out using our home-made electrospinning system. The schematic diagram of electrospinning process is shown in Fig. 1. The needle was connected to a high-voltage supply and for each solution the voltage of 18 kV was applied. The solution was fed at a rate of 1.0 mL/h using a motor syringe pump. A piece of flat aluminum foil was placed 15 cm below the tip of the needle, and used to collect the nanofibers. All electrospinning processes were carried out at room temperature.

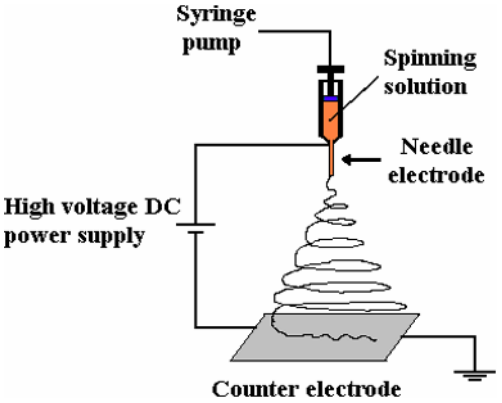

Fig. 1 Schematic diagram of electrospinning set up

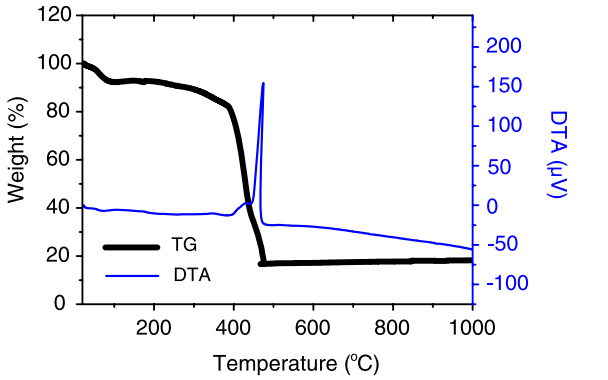

Fig. 2 TG-DTA curves of thermal decomposition of the as-spun $CoFe_2O_4$/PVP composite sample at a heating rates of 5°C/min in static air

The as-spun $CoFe_2O_4$/PVP composite nanofibers were subjected to thermogravimetric-differential thermal analysis (TG-DTA) using Pyris Diamond TG/DTA (PerkinElmer Instrument, USA). This was done to determine the temperatures of possible decomposition and crystallization (or phase changes) of the as-spun nanofibers. The analyses were performed with a heating rate of 5°C/min in static air up to 1000°C. The composite nanofibers were calcined at 500, 600, and 800°C for 3 h in air in box furnace (Lenton Furnaces, U.K.), using either heating and cooling rates of 5°C/min or 20 min/°C. The final products obtained were dark brown $CoFe_2O_4$ samples. The as-spun and calcined nanofibers were characterized by means of X-ray diffraction (XRD) using CuK_α radiation with $\lambda = 0.15418$ nm (PW3040 mpd control, The Netherlands), FT-IR spectroscopy (Spectrum One FT-IR Spectrometer, PerkinElmer Instruments, USA), scanning electron microscopy (SEM) (LEO VP1450, U.K. and Hitachi FE-SEM S-4700, Japan) and transmission electron microscopy (TEM) (JEOL TEM 2010, Japan). The average diameter of the as-spun composite nanofibers was determined from about 300 measurements. The magnetic properties of the calcined samples were examined at room temperature (20°C) using a vibrating sample magnetometer (VSM) (Lake Shore VSM 7403, USA).

3 Results and discussion

The TG curve in Fig. 2 shows a minor weight loss (∼18%) step from 30°C up to about 380°C and a major weight loss (∼64%) step from 380°C up to about 475°C with no weight loss observed up to 1000°C. The minor weight loss was related to the loss of moisture and trapped solvent (water, ethanol and carbon dioxide) in the as-spun nanofibers while the major weight loss was due to the combustion of organic PVP matrix. On the DTA curve, a main exothermic peak was observed at ∼470°C, suggesting the thermal events related to the decomposition of Co and Fe nitrates along with the degradation of PVP by a dehydration on the polymer side chain, which was confirmed by a dramatic weight loss in TG curve at the corresponding temperature range (380–475°C). The plateau formed between 320 and 1000°C on the TG curve indicated the formation of nanocrystalline $CoFe_2O_4$ as the decomposition product [28, 36], as confirmed by selected area electron diffraction (SAED) in TEM, XRD and FT-IR analyses shown in Figs. 6, 7, and 8, respectively.

Figure 3 shows morphology and fiber diameter distribution of the as-spun $CoFe_2O_4$/PVP composite nanofibers. Figure 3a is a digital camera photograph showing a sheet of $CoFe_2O_4$/PVP composite nanofibers taken out from aluminum foil, while Fig. 3b–3e show the SEM micrographs of the as-spun $CoFe_2O_4$/PVP composite nanofibers at magnifications of ×1000 (Fig. 3b), ×5000 (Fig. 3c), ×10000 (Fig. 3d), ×30000 (Fig. 3e) with the respective diameter histograms (Fig. 3f). The as-spun composite nanofibers appeared quite smooth due to the amorphous nature of $CoFe_2O_4$/PVP composite (Fig. 3b–3e). Each individual nanofiber was quite uniform in cross section, and the average diameter of the fibers was 320 ± 48 nm.

The PVP was selectively removed by calcination the as-spun composite nanofibers in air at above 500°C. Figures 4, and 5 show the SEM micrographs of the $CoFe_2O_4$/PVP composite nanofibers calcined at 500, 600, and 800°C with different heating rates of 5°C/min (Fig. 4) and 20°C/min (Fig. 5). It is seen from Fig. 4 that the composite nanofibers calcined at 500, 600, 800°C with a heating rate of 5°C/min remained as continuous structures (Figs. 5a–3c), and their diameters appeared to be decreased to 100–200 nm. The reduction in size of the nanofibers should be attributed to the loss of PVP from the nanofibers and the crystallization of $CoFe_2O_4$. After calcination at 800°C, the nature of nanofibers was dramatically changed, and a structure of packed particles or crystallites was prominent. These changes in the morphology are related to a dramatic change in crystal structure as observed in electrospun $NaCo_2O_4$

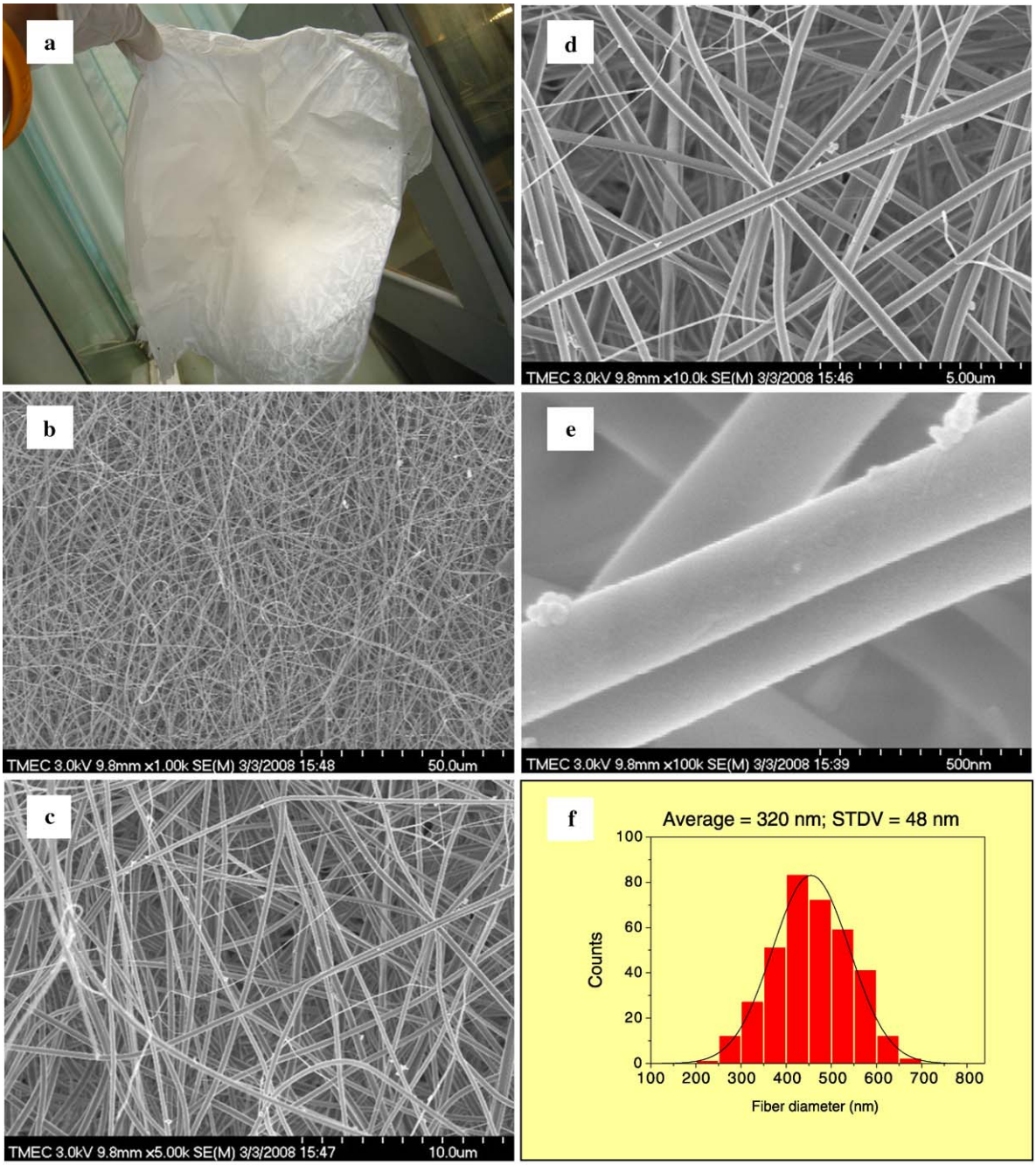

Fig. 3 Morphology and fiber diameter distribution of the as-spun $CoFe_2O_4$/PVP composite sample. (**a**) Digital photograph, (**b**) ×1000 SEM image, (**c**) ×5000 SEM image, (**d**) ×10000 SEM image, (**e**) ×30000 SEM image, and (**f**) fiber diameter distribution

[35], $Ba_{0.6}Sr_{0.4}TiO_3$ [36], $CuFe_2O_4$ [39], and $MgFe_2O_4$ [40]. The particle sizes of composite nanofibers calcined at 500, 600, and 800°C were ∼<10, 10–20, and 50–200 nm in diameter, respectively. For the composite nanofibers calcined at 500, 600, 800°C with a heating rate of 20°C/min (Fig. 5), the nature of nanofibers dramatically changed. The 500°C-calcined composite nanofibers remained as continuous structures with a fiber structure of packed particles or crystallites, whereas the 600°C- and 800°C-calcined composite nanofibers became fine particles with particle sizes of 50–100 nm and 200–400 nm, respectively. It is clear from these results that heating rate has a strong effect on morphology of the calcined $CoFe_2O_4$/PVP composite nanofibers. A faster heating rate would allow for a rapid removal of the PVP matrix and results in a complete change from fibrous structure to particle in the calcined $CoFe_2O_4$/PVP composite nanofibers. Therefore, we can control the formation of either fibrous structure or nanoparticle of electrospun

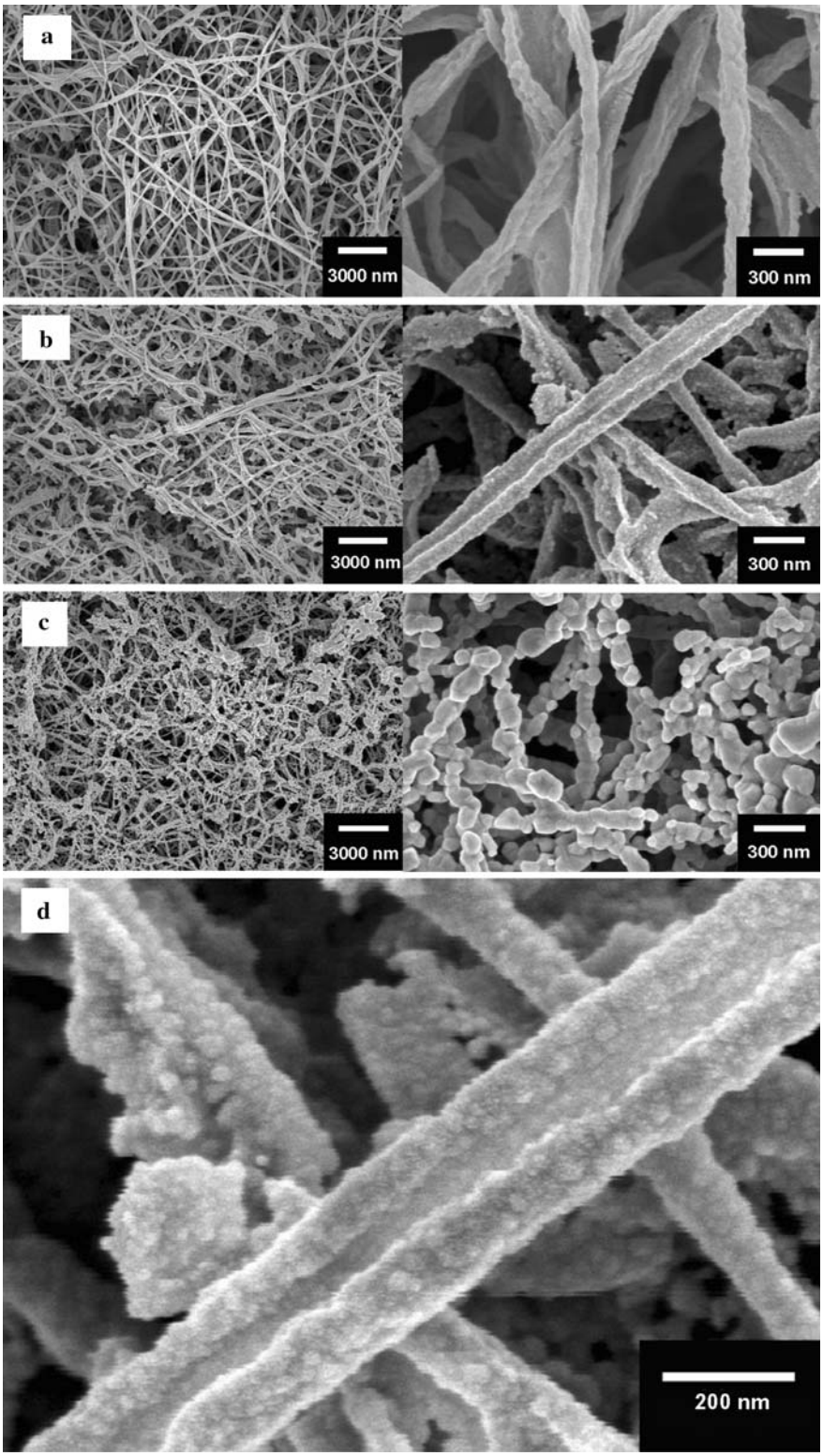

Fig. 4 SEM micrographs of the $CoFe_2O_4$/PVP composite samples calcined in air for 3 h with heating rate of 5°C/min at different temperatures: (**a**) and (**d**) 500°C, (**b**) 600°C, and (**c**) 800°C. High magnification SEM image in (**d**) shows the structure of linked particles or crystallites of <20 nm in size

$CoFe_2O_4$/PVP composite nanofibers by varying the heating rate during the calcination process.

The detailed morphology and crystalline structure of the composite nanofibers calcined at 500, 600, 800°C with heating rate of 20°C/min composite nanofibers were further investigated by TEM. Figure 6 shows TEM bright-field images with corresponding selected-area electron diffraction (SAED) patterns of the $CoFe_2O_4$/PVP composite nanofibers calcined in air for 3 h at different temperatures. It is clearly seen from the TEM bright-field images (Fig. 6) that the mor-

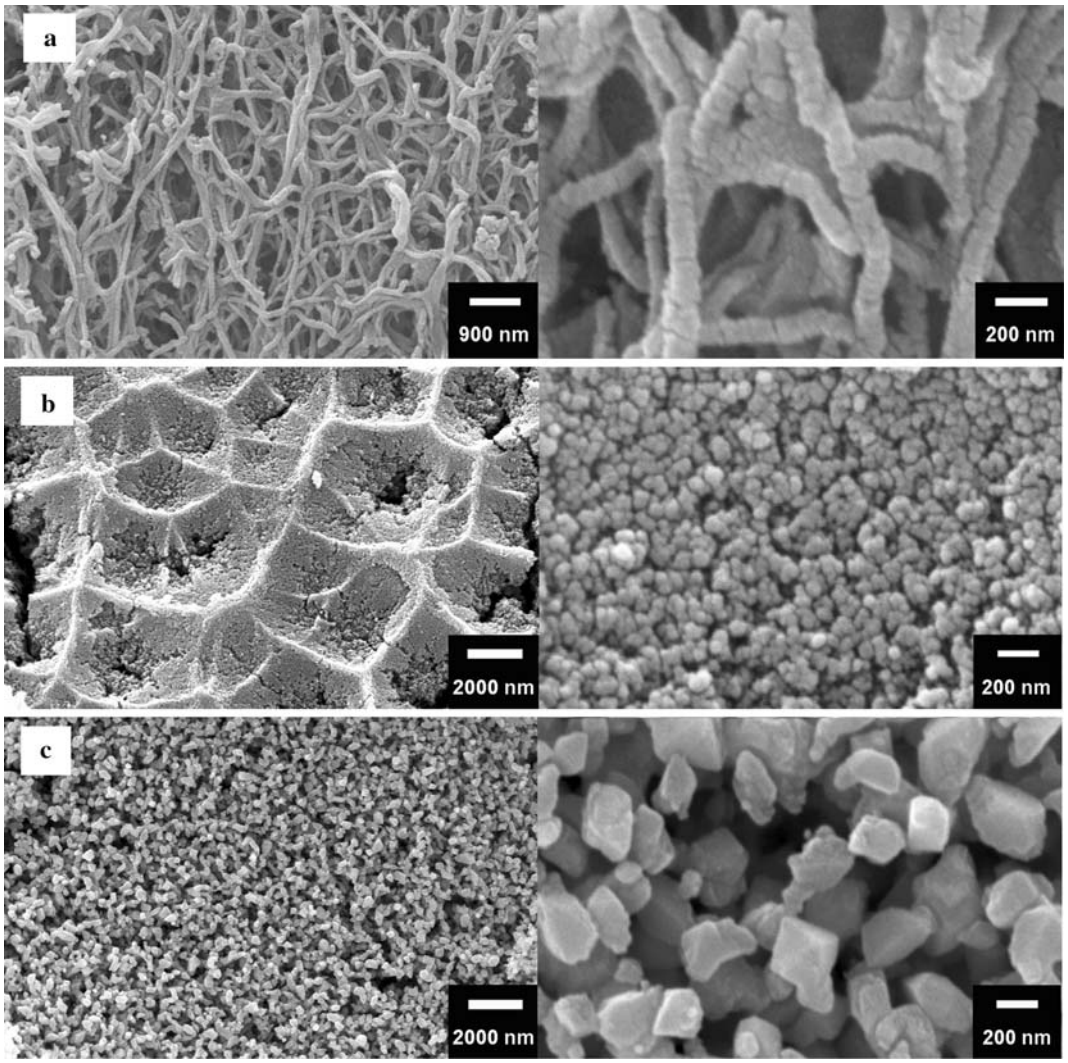

Fig. 5 SEM micrographs of the $CoFe_2O_4$/PVP composite nanofibers calcined in air for 3 h with heating rate of 20°C/min at temperatures of (**a**) 500°C, (**b**) 600°C, and (**c**) 800°C

phology and size of the materials were significantly affected by the calcination temperature. The 500°C-calcined composite nanofibers remained as continuous structures with a fiber structure of packed particles or crystallites with a size of <10 nm, whereas the 600°C- and 800°C-calcined composite nanofibers became an agglomerate of fine particles with particle sizes of 10–20 nm and 50–200 nm, respectively. It is worth noting that the particle sizes of $CoFe_2O_4$ contained in the 500°C-calcined composite nanofibers are quite uniform. This might have resulted from the rates of hydrolysis involved in the fabrication process, in which the water required for the hydrolysis of metal precursors was supplied by the moisture in air [38–40]. Since the electrospun fibers were very small in diameter, the moisture could quickly diffuse into the fibers, causing a rapid and uniform hydrolysis of the metal precursors. The corresponding selected-area electron diffraction (SAED) patterns (Fig. 6) of all the $CoFe_2O_4$/PVP composite nanofibers show spotty ring patterns, revealing their crystalline spinel $CoFe_2O_4$ structure. Increase in calcination temperature results in a stronger spotty pattern and the $CoFe_2O_4$/PVP composite nanofibers calcined at 800°C shows strongest spotty patterns, indicating large crystallite of highly crystalline spinel structure. According to the diffraction patterns in Fig. 6, the measured lattice constants agree with those in the XRD results and the standard data (JCPDS: 22-1086). Measured interplanar spacings (d_{hkl}) from selected-area electron diffraction patterns in Fig. 6 are in good agreement with the values in the standard data (JCPDS: 22-1086).

The XRD patterns of the $CoFe_2O_4$/PVP composite nanofibers calcined at 500, 600, and 800°C with different heating rates of 5 and 20°C/min are shown in Fig. 7. All of the main peaks are indexed as the $CoFe_2O_4$ with spinel structure as shown in the standard data (JCPDS:

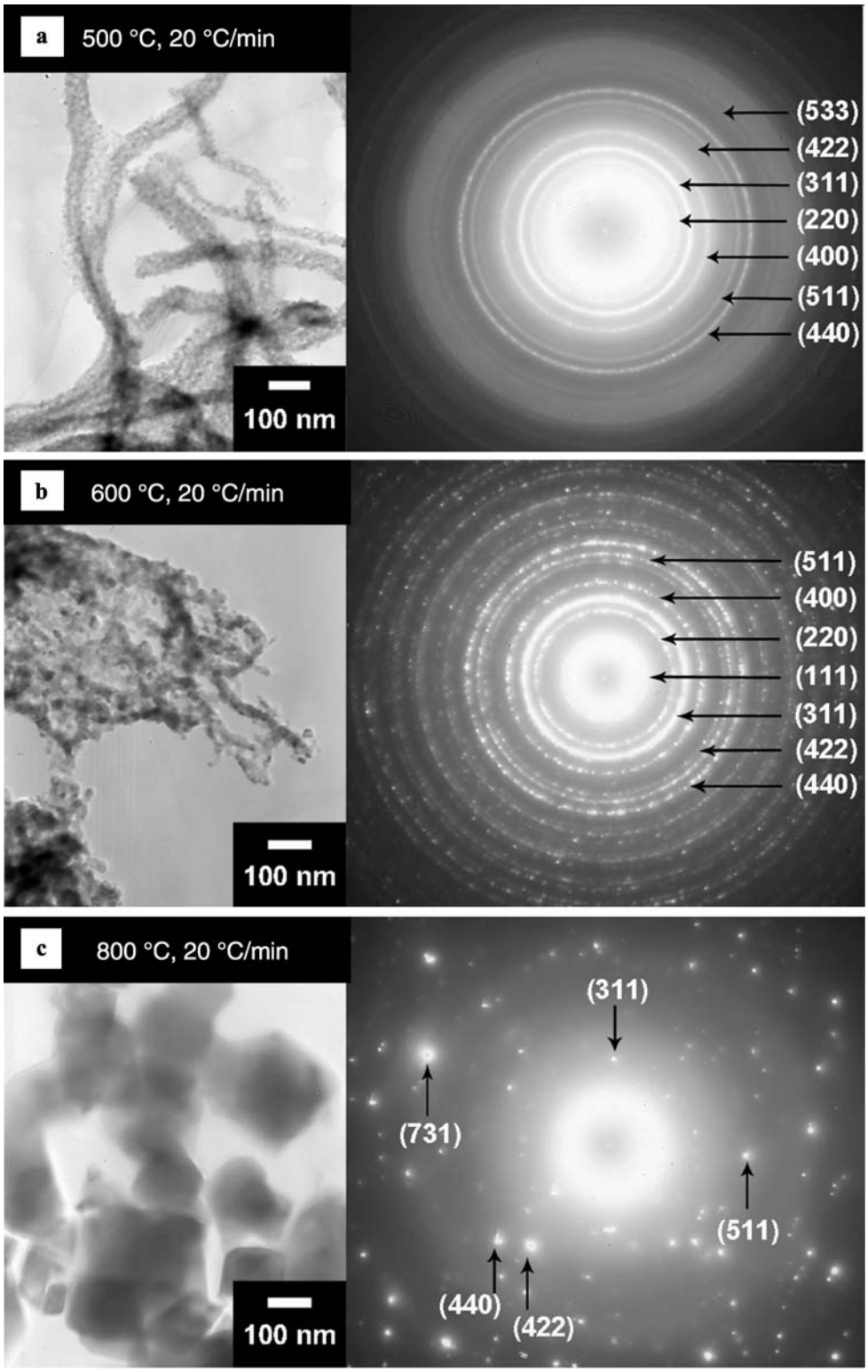

Fig. 6 TEM images with corresponding selected area electron diffraction patterns of the $CoFe_2O_4$/PVP composite samples calcined in air for 3 h with heating rates of 20°C/min at temperatures of (**a**) 500°C, (**b**) 600°C, and (**c**) 800°C

10-0325). However, peaks of impurities at $2\theta \approx 26.5$ and 34 degree were observed in the $CoFe_2O_4$/PVP composite nanofibers calcined at 800°C with heating rate of 20°C/min. It is clearly seen that the reflection peaks become sharper and narrower along with the increasing of calcination temperatures, indicating the enhancement of crystallinity. The average crystallite sizes of the calcined $CoFe_2O_4$/PVP composite nanofibers were calculated from X-ray line broadening of the reflections of (220), (311), (400), (422), (511) and (440) using Scherrer's equation (i.e. $D = K\lambda/(\beta \cos\theta)$,

Table 1 Average crystal sizes from XRD, spinel lattice parameter a calculated from XRD spectra, the specific magnetization (M_s), remnant magnetization (M_r), the ratio of the ratio of remnant magnetization to bulk saturation magnetization (M_r/M_s), and coercive forces (H_c) of the $CoFe_2O_4$/PVP composite samples calcined in air for 3 h at different temperatures and heating rates

$CoFe_2O_4$/PVP sample	Average crystallite size from XRD (nm)	Spinel lattice parameter a (nm)	M_s (emu/g) at 10 kOe	M_r (emu/g)	M_r/M_s	H_c (Oe)	Estimated region of hysteresis (Oe)
500°C, 5°C/min	29 ± 4	0.8353 ± 0.0011	56.5	24.9	0.44	1117.2	±4500
600°C, 5°C/min	33 ± 6	0.8347 ± 0.0011	61.9	28.8	0.47	1185.4	±4500
800°C, 5°C/min	38 ± 3	0.8355 ± 0.0010	71.7	35.9	0.50	860.6	±4500
500°C, 20°C/min	27 ± 2	0.8344 ± 0.0017	9.7	1.5	0.15	241.6	±3000
600°C, 20°C/min	30 ± 5	0.8349 ± 0.0011	33.9	7.7	0.23	441.9	±3000
800°C, 20°C/min	54 ± 4	0.8341 ± 0.0018	61.8	31.1	0.50	655.4	±3000

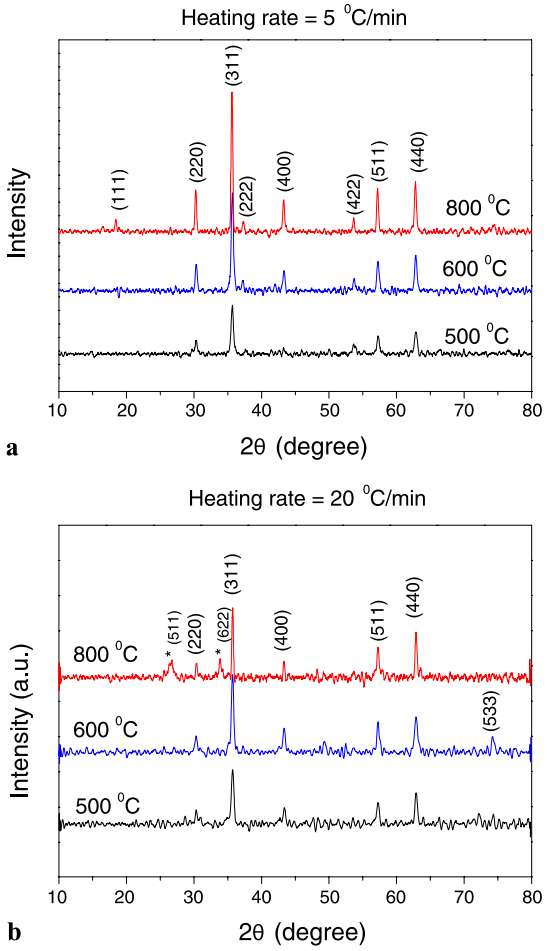

Fig. 7 XRD patterns of the as-spun $CoFe_2O_4$/PVP composite sample and $CoFe_2O_4$/PVP composite samples calcined in air for 3 h at different temperatures and heating rates. (**a**) heating rate of 5°C/min, (**b**) heating rate of 20°C/min

where λ is the wavelength of the X-ray radiation, K is a constant taken as 0.89, θ is the diffraction angle and β is the full width at half maximum (FWHM) [41]), and were found to be 29 ± 4, 33 ± 6 and 38 ± 3 nm for the samples of $CoFe_2O_4$/PVP composite nanofibers calcined respectively at 500, 600, and 800°C with heating rate of 5°C/min, and to be 27 ± 2, 30 ± 5 and 54 ± 4 nm for the samples of $CoFe_2O_4$/PVP composite nanofibers calcined respectively at 500, 600, and 800°C with heating rate of 20°C/min. The values of the lattice parameter a calculated from the XRD spectra were 0.8353 ± 0.0011, 0.8347 ± 0.0011 and 0.8355 ± 0.0010 nm for the samples of $CoFe_2O_4$/PVP composite nanofibers calcined respectively at 500, 600, and 800°C with heating rate of 5°C/min, and to be 0.8344 ± 0.0017, 0.8349 ± 0.0011 and 0.8341 ± 0.0018 nm for the samples of $CoFe_2O_4$/PVP composite nanofibers calcined respectively at 500, 600, and 800°C with heating rate of 20°C/min. The values of the lattice parameter a are slightly smaller than that reported for $CoFe_2O_4$ ($a = 0.83919$ nm) in the standard data (JCPDS: 22-1086). The crystallite sizes and lattice parameters are also summarized in Table 1.

The formation of spinel structure in the $CoFe_2O_4$/PVP composite nanofibers calcined at 500, 600, and 800°C with heating rate of 20°C/min was further supported by FTIR spectra (Fig. 8). Here we consider two ranges of the absorption bands: 4000–1000 cm^{-1} and 1000–400 cm^{-1} as suggested by previously published works [42–44]. In the range of 4000–1000 cm^{-1}, vibrations of CO_3^{2-}, NO_3^- and moisture are observed. The intensive broadband at ~(3432–3438) cm^{-1} and the less intensive band at ~(1629–1655) cm^{-1} are due to O–H stretching vibration interacting through H bonds. The band at ~(2927–2933) cm^{-1} is the C–H asymmetric stretching vibration mode due to the $–CH_2–$ groups of the long aliphatic alkyl groups. The presence of a small band at ~(2307–2377) is due to atmospheric CO_2, which has been adsorbed on the surface of the sample during the preparation of the pellets. The ν(C=O) stretching

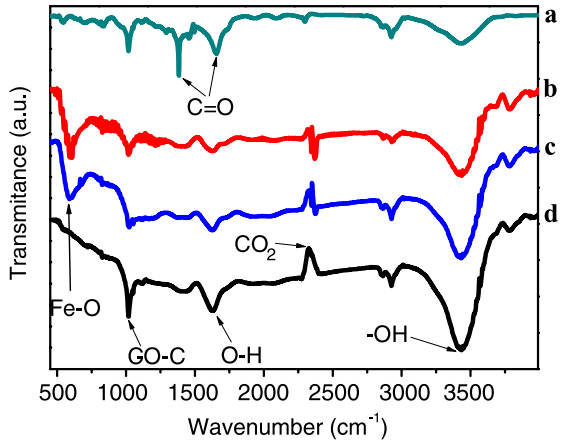

Fig. 8 FT-IR spectra of the as-spun $CoFe_2O_4$/PVP composite sample and $CoFe_2O_4$/PVP composite samples calcined in air for 3 h with heating rates of 20°C/min at temperatures of (**a**) 500°C, (**b**) 600°C, and (**c**) 800°C

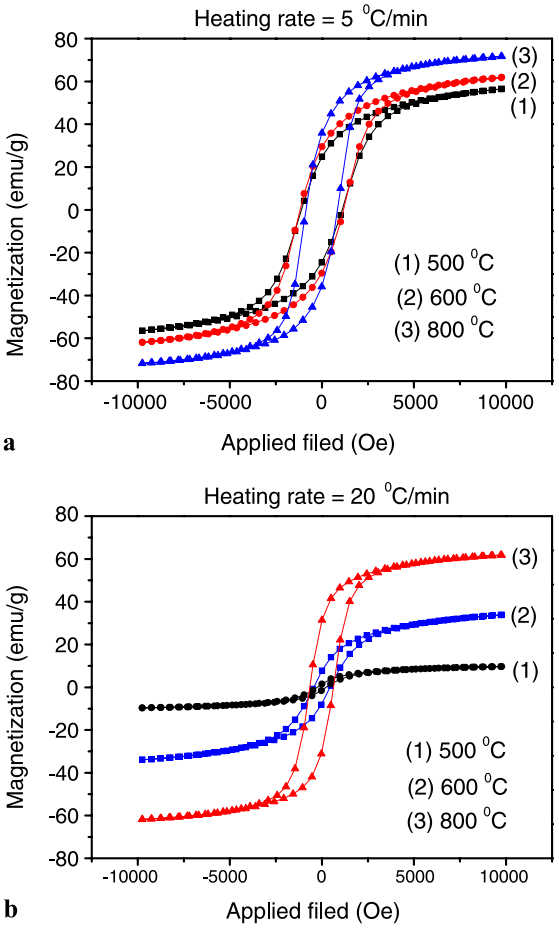

Fig. 9 The specific magnetization of the $CoFe_2O_4$/PVP composite samples calcined in air for 3 h at different temperatures and heating rates, as a function of field, measured at 20°C: (**a**) heating rate of 5°C/min, (**b**) heating rate of 20°C/min. (*1*), (*2*), and (*3*) are the samples calcined in air for 3 h at 500, 600, and 800°C, respectively

vibration of the carboxylate group (CO_2^-) is observed at ∼(1380–1387) cm^{-1} and the band at ∼(1019–1022) cm^{-1} corresponds to nitrate ion traces. Therefore, the CO_3^{2-} and CO_2^- vibrations tend to disappear if the calcination temperature is increased. In the range of 1000–400 cm^{-1}, the typical metal-oxide vibration band characteristic of $CoFe_2O_4$ (∼(543–594) corroborating the spinel structure characteristics of $CoFe_2O_4$ is observed in the FTIR spectra of all of the calcined samples of $CoFe_2O_4$/PVP composite nanofibers. The band at ∼(543–594) cm^{-1} strongly suggests the intrinsic stretching vibrations of the metal (Fe ↔ O) at the tetrahedral site [44].

The specific magnetization curves of the calcined $CoFe_2O_4$/PVP composite nanofibers obtained from room temperature VSM measurement are shown in Fig. 9. These curves are typical for a soft magnetic material and indicate hysteresis ferromagnetism in the field range of ±4500 Oe and ±3000 Oe for $CoFe_2O_4$/PVP composite nanofibers calcined respectively with heating rates of 5 and 20°C/min, while outside this range the specific magnetization increases with increasing field and tends to saturate in the field range investigated (±10 kOe). The specific saturation magnetization (M_s) values were obtained to be 56.5, 61.9, and 71.7 emu/g at 10 kOe for the samples of $CoFe_2O_4$/PVP composite nanofibers calcined respectively at 500, 600, and 800°C with heating rate of 5°C/min, and to be 9.7, 33.9, and 61.8 emu/g at 10 kOe for the samples of $CoFe_2O_4$/PVP composite nanofibers calcined respectively at 500, 600, and 800°C with heating rate of 20°C/min.

It is found that the increase of the tendency of M_s is consistent with the enhancement of crystallinity, and the values of M_s for the calcined $CoFe_2O_4$ samples were observed to increase with increasing crystallite size. It is noted that the saturation values of 61.9 and 61.8 emu/g obtained in the samples of $CoFe_2O_4$/PVP composite nanofibers calcined at 600°C with heating rate of 5°C/min (crystallite size of 33 ± 6 nm) and calcined at 800°C with heating rate of 20°C/min (crystallite size of 54 ± 4 nm) are comparable to the reported values of ∼65 emu/g for the $CoFe_2O_4$ nanoparticles with crystallite size of ∼40 nm prepared by aerosol route [45]. The values of M_s for the calcined samples of $CoFe_2O_4$/PVP composite nanofibers are observed to increase with increasing crystallite size. This can be explained by considering a magnetic domain of the samples [46]. Since the energy of a magnetic particle in an external filed is proportional to its particle size via the number of magnetic molecules in a single magnetic domain, the particle size will be increased and the crystallization will be more complete with increasing calcination temperature. Moreover, the magnetic phase will be increased because the cubic spinel structure is purer and more complete with the absorption of higher thermal energy. Thus, the larger particle or crystallite size leads to the higher value of the specific mag-

netization. It is worth noting that calcination temperature and heating rate not only affect the morphology and structure but also the magnetic properties of $CoFe_2O_4$/PVP composite nanofibers. Slower heating rate of calcination leads to larger M_s in the $CoFe_2O_4$/PVP composite nanofibers. We cannot yet clearly explain this, but it is possible that calcination with slower heating rate allows the crystallization to be more complete and magnetic phase also increases which results in larger M_s.

From Fig. 9, the remnant magnetization (M_r) values were obtained to be 24.9, 28.8, and 35.9 emu/g for the samples of $CoFe_2O_4$/PVP composite nanofibers calcined respectively at 500, 600, and 800°C with heating rate of 5°C/min, and to be 1.5, 7.7, and 31.1 emu/g for the samples of $CoFe_2O_4$/PVP composite nanofibers calcined respectively at 500, 600, and 800°C with heating rate of 20°C/min. As a result, the ratios of remnant magnetization to bulk saturation magnetization, M_r/M_s, were obtained to be 0.44, 0.47, and 0.50 for the samples of $CoFe_2O_4$/PVP composite nanofibers calcined respectively at 500, 600, and 800°C with heating rate of 5°C/min, and to be 0.15, 0.23, and 0.50 for the samples of $CoFe_2O_4$/PVP composite nanofibers calcined respectively at 500, 600, and 800°C with heating rate of 20°C/min. These results are not consistent with results obtained on ferromagnetic nanoparticles reported in the literature [47, 48]. For ferromagnetic nanoparticles, it is interesting to note that the magnetization is strongly dependent on their particle size, as shown by an electron holography study of carbon-coated Ni and Co nanoparticles [47]. The ratio of remnant magnetization to bulk saturation magnetization, M_r/M_s, of Co decreased from 53% to 16% and of Ni decreased from 70% to 30% as the particle diameter increased from 25 to 90 nm. In the case of egg white synthesized $NiFe_2O_4$ nanoparticles [48], the ratio of M_r/M_s decreased from 14.8% to 3.8% as the particle diameter increased from 54 to 107 nm. It is clearly seen from these two reports that the smaller the particles the higher the remnant magnetization. This is due to the tendency of smaller particles to be a single magnetic domain, and larger particles usually contain multiple domains. At present, we cannot explain the difference in the M_r/M_s values obtained in our calcined $CoFe_2O_4$/PVP composite nanofibers. However, it is possible that the magnetic shape anisotropy plays an important role and further work is needed to achieve a thorough understanding.

The coercive forces (H_c) were obtained to be 1117.2, 1185.4, and 860.6 Oe for the samples of $CoFe_2O_4$/PVP composite nanofibers calcined respectively at 500, 600, and 800°C with heating rate of 5°C/min, and to be 241.6, 441.9, and 655.4 Oe for the samples of $CoFe_2O_4$/PVP composite nanofibers calcined respectively at 500, 600, and 800°C with heating rate of 20°C/min. It is known that the variation of H_c with particle size can be explained on the basis of domain structure, critical diameter and the anisotropy of the crystal [49–52]. It has been reported [46] that the larger size of $CoFe_2O_4$ particles leads to the higher values of both specific magnetization and coercivity. Considering this together with the experimental results obtained in this study, the samples of $CoFe_2O_4$/PVP composite nanofibers calcined with heating rates of 5 and 20°C/min exhibit behavior similar to that reported in Ref. 45, except the sample calcined at 800°C with heating rate of 5°C/min that the effect of the crystallite size on the low coercivity of this sample may be ruled out. We think that the decrease in anisotropy field, which in turn decreases the domain wall energy, is more likely the mechanism responsible for the low coercivity of the $CoFe_2O_4$/PVP composite nanofibers calcined at 800°C. However, further work on the study of magnetic anisotropy is needed to achieve thorough understanding. The values of specific magnetization at 10 kOe, remnant magnetization (M_r), the ratio of remnant magnetization to bulk saturation magnetization (M_r/M_s), and coercive forces (H_c) are also tabulated in Table 1.

4 Conclusion

Nanofibers and nanoparticles of $CoFe_2O_4$ have been successfully fabricated using an electrospinning technique. After calcination of the as-spun $CoFe_2O_4$/PVP composite nanofibers (fiber size of 320 ± 48 nm in diameter) at 500–800°C in air for 3 h with different heating rates of 5 or 20°C/min, either $CoFe_2O_4$ nanofibers of $\sim$10−200 nm in diameter (with packed particles or crystallite sizes of $\sim$29−50 nm) or nanoparticles with particle sizes of $\sim$50−400 nm having well-developed spinel structure were successfully obtained, as confirmed by XRD, FT-IR and SAED analysis. The crystal structure and morphology of the nanofibers were influenced by the calcination temperature and heating rate. All the calcined samples of the $CoFe_2O_4$/PVP composite nanofibers exhibited ferromagnetism, having their hysteresis loops in the field range of $\pm$4500 and 3000 Oe for the samples calcined respectively with heating rates of 5 and 20°C/min. The values of M_s at 10 kOe, M_r, M_r/M_s ratio, and H_c were in the ranges of 9.7–61.9 emu/g, 1.5–35.99 emu/g, 2.0–6.5, and 241.6–1185.4 Oe, depending on calcination temperature and heating rate. This work demonstrates that we can control the formation of either fibrous structure or nanoparticle of electrospun $CoFe_2O_4$/PVP composite nanofibers and their resulting magnetic properties by varying heating rate during the calcination process. We believe that the electrospun $CoFe_2O_4$ nanostructures would have potential in some new applications as ferromagnetic fibers for nanocomposites, separation, anodic material in lithium ion batteries, catalysts, and as electronic material for nanodevices and storage devices.

Acknowledgement The authors would like to thank the Department of Chemistry for providing TG-DTA, FTIR and VSM facilities, SEM unit of Faculty of Science for SEM facilities, the Science and Technology Service Center (Chiang Mai University) for providing TEM facilities, Department of Physics, Faculty of Science, Ubon Ratchathani University for providing XRD facilities, and the Thai Microelectronics Center (TMEC) for FE-SEM facilities. This work is partially supported by The National Nanotechnology Center (NANOTEC), NSTDA, Ministry of Science and Technology, Thailand, through its program of Center of Excellence.

References

1. M. Sugimoto, J. Am. Ceram. Soc. **82**, 269 (1999)
2. R.C. O'Handley, *Modern Magnetic Materials—Principles and Applications* (Wiley, New York, 2001)
3. R. Valenzuela, *Magnetic Ceramics* (Cambridge University Press, Cambridge, 1994)
4. E. Matijevic, MRS Bull. **12**, 19 (1989)
5. E.S. Murdock, IEEE Trans. Magn. **28**, 3078 (1992)
6. S.N. Okuno, S. Hashimotos, K. Inomata, J. Appl. Phys. **71**, 5926 (1992)
7. K. Ozaki, MRS Bull. **12**, 35 (1989)
8. A.K. Giri, K. Pellerin, W. Pongsaksawad, M. Sorescu, S. Majetich, IEEE Trans. Magn. **36**, 3029 (2000)
9. A.K. Giri, E.M. Kirkpatrick, P. Moongkhamklang, S.A. Majetich, V.G. Harris, Appl. Phys. Lett. **80**, 2341 (2002)
10. R.N. Singh, N.K. Singh, J.P. Singh, Electrochim. Acta **47**, 3873 (2002)
11. X.H. Yang, X. Wang, Z.D. Zhang, J. Cryst. Growth **277**, 467 (2005)
12. X. Chu, D. Jiang, Y. Guo, C. Zheng, Sens. Actuator B **120**, 177 (2006)
13. C.C. Wang, I.H. Chen, C.R. Lin, J. Magn. Magn. Mater. **304**, e451 (2006)
14. S.W. Lee, C.S. Kim, J. Magn. Magn. Mater. **303**, e315 (2006)
15. P.D. Thang, G. Rijnders, D.H.A. Blank, J. Magn. Magn. Mater. **310**, 2621 (2007)
16. Z.H. Hua, R.S. Chen, C.L. Li, S.G. Yang, M. Lu, B.X. Gu, Y.W. Du, J. Alloys Compd. **427**, 199 (2007)
17. K. Maaz, A. Mumtaz, S.K. Hasanain, A. Ceylan, J. Magn. Magn. Mater. **308**, 289 (2007)
18. G. Ji, S. Tang, B. Xu, B. Gu, Y. Du, Chem. Phys. Lett. **379**, 484 (2003)
19. D.H. Renaker, I. Chun, Nanotechnology **7**, 216 (1996)
20. A. Frenot, I.S. Chronakis, Curr. Opin. Colloid. Interface Sci. **8**, 64 (2003)
21. Z.H. Huang, Y.Z. Zhang, M. Kotaki, S. Ramakrishna, Compos. Sci. Technol. **63**, 2223 (2003)
22. D. Li, Y. Xia, Adv. Mater. **16**, 1151 (2004)
23. D.H. Reneker, A.L. Yarin, H. Fong, S. Koombhonge, J. Appl. Phys. **87**, 4531 (2000)
24. A.L. Yarin, S. Koombhongse, D.H. Reneker, J. Appl. Phys. **89**, 3018 (2001)
25. A.L. Yarin, D.H. Reneker, J. Appl. Phys. **90**, 4836 (2001)
26. G.C. Rutledge, S.V. Fridrikh, Adv. Drug Deliv. Rev. **59**, 1384 (2007)
27. D. Li, Y. Wang, Y. Xia, Nano Lett. **3**, 555 (2003)
28. W. Naunsing, S. Ninmuang, W. Jarernboon, S. Maensiri, S. Seraphin, Mater. Sci. Eng. B **131**, 147 (2006)
29. P. Viswanathamurthi, N. Bhattarai, H.Y. Kim, D.R. Lee, Scr. Mater. **49**, 577 (2003)
30. P. Viswanathamurthi, N. Bhattarai, H.Y. Kim, D.R. Lee, Nanotechnology **15**, 320 (2004)
31. H. Guan, C. Shao, Y. Liu, N. Yu, X. Yang, Solid State Commun. **131**, 107 (2004)
32. N. Dharmaraj, H.C. Park, B.M. Lee, P. Viswanathamurthi, H.Y. Kim, D.R. Lee, Inorg. Chem. Commun. **7**, 431 (2004)
33. N. Yu, C. Shao, Y. Liu, H. Guan, X. Yang, J. Colloid Interface Sci. **285**, 163 (2005)
34. Y. Wang, J.J. Santiago-Aviles, Nanotechnology **15**, 32 (2004)
35. S. Maensiri, W. Nuansing, Mater. Chem. Phys. **99**, 104 (2006)
36. S. Maensiri, W. Nuansing, J. Klinkaewnarong, P. Laokul, J. Khemprasit, J. Colloid Interface Sci. **297**, 578 (2006)
37. M. Liao, X.L. Zhong, J.B. Wang, H.L. Yan, J.P. He, Y. Qiao, Y.C. Zhou, J. Cryst. Growth **304**, 69 (2007)
38. D. Li, T. Herricks, Y. Xia, Appl. Phys. Lett. **83**, 4586 (2003)
39. W. Ponhan, S. Maensiri, Solid State Sci. **11**, 479 (2009)
40. S. Maensiri, M. Saengmanee, A. Wiengmoon, Nanoscale Res. Lett. **4**, 221 (2009)
41. B.D. Cullity, S.R. Stock, *Elements of X-ray Diffraction*, 3rd edn. (Printice-Hall, Englewood Cliffs, 2001)
42. C. Cannas, A. Falqui, A. Musinu, D. Peddis, G. Piccaluga, J. Nanopart. Res. **8**, 255 (2006)
43. D.-E. Zhang, X. Zhang, X.-M. Ni, J.-M. Song, H.-G. Zheng, J. Magn. Magn. Mater. **305**, 68 (2006)
44. R.D. Waldron, Phys. Rev. **99**, 1727 (1955)
45. S. Singhal, J. Singh, S.K. Barthwal, K. Chandra, J. Solid State Chem. **178**, 3183 (2005)
46. L. Zhao, H. Yang, X. Zhao, Y. Yu, Y. Cui, S. Feng, Mater. Lett. **60**, 1 (2006)
47. S. Seraphin, C. Beeli, J.-M. Bonard, J. Jiao, P.A. Stadelmann, A. Chatelain, J. Mater. Res. **14**, 2861 (1999)
48. S. Maensiri, C. Masingboon, B. Boonchom, S. Seraphin, Scr. Mater. **56**, 797 (2006)
49. B.D. Cullity, *Introduction to Magnetic Materials* (Addison-Wesley, Reading, 1972)
50. S. Chikazumi, *Physics of Magnetism* (Wiley, New York, 1959)
51. M. Georgea, A. Mary John, S.S. Naira, P.A. Joy, M.R. Anantharaman, J. Magn. Magn. Mater. **302**, 190 (2006)
52. Y.M. Yakovlev, E.Y. Rubalikaya, N. Lapovok, Sov. Phys. Solid State **10**, 2301 (1969)